Journal of Systems Engineering and Electronics
Vol. PP, No. 99, July 2023, pp.1 – 9

Unconditionally stable Crank-Nicolson algorithm with enhanced absorption for rotationally symmetric multi-scale problems in anisotropic magnetized plasma

WEN Yi [1,2,*], WANG Junxiang [2], and XU Hongbing [1]

1. School of Automatic Engineering, University of Electronic Science and Technology of China, Chengdu 611731, China;
2. Beijing Institute of Aerospace Systems Engineering, Beijing 100076, China

Abstract: Large calculation error can be formed by directly employing the conventional Yee 's grid to curve surfaces. In order to alleviate such condition, unconditionally stable Crank-Nicolson Douglas-Gunn (CNDG) algorithm with is proposed for rotationally symmetric multi-scale problems in anisotropic magnetized plasma. Within the CNDG algorithm, an alternative scheme for the simulation of anisotropic plasma is proposed in body-of-revolution domains. Convolutional perfectly matched layer (CPML) formulation is proposed to efficiently solve the open region problems. Numerical example is carried out for the illustration of effectiveness including the efficiency, resources, and absorption. Through the results, it can be concluded that the proposed scheme shows considerable performance during the simulation.

Keywords: anisotropic magnetized plasma, body-of-revolution (BOR), Crank-Nicolson Douglas-Gunn (CNDG), finite-difference time-domain (FDTD), perfectly matched layer (PML), rotationally symmetric multi-scale problems.

DOI: 10.23919/JSEE.2023.000072

1. Introduction

Finite-difference time-domain (FDTD) algorithm can be regarded as one of the most important methods in solving the Maxwell's equations [1]. During the development of FDTD algorithm, several problems should be further investigated including multi-scale problems, conformal techniques, and open region problems [2−4].

By applying the conventional FDTD algorithm to the curve surfaces, large calculation error will be formed due to the introduction of mesh conformal technique [5]. In order to alleviate such condition, body-of-revolution FDTD (BOR-)FDTD algorithm is proposed for the simulation of rotationally symmetric structures [6]. According to the BOR-FDTD algorithm, three-dimensional problems can be converted to two-dimensional problems resulting in the improvement of efficiency and resources [7,8]. However, the original BOR-FDTD algorithm is still a time-explicit algorithm whose stability is severely limited by the Courant-Friedrichs-Levy (CFL) condition [9]. This means that the established relationship is formed between the time step and mesh size. By applying such scheme directly to multi-scale problems, mesh size is selected according to the fine details resulting in extremely large domain and long time duration. To alleviate such condition, unconditionally stable algorithms are proposed to overcome the stability condition and improve the efficiency which include the alternating direction implicit (ADI), locally one-dimensional (LOD) and split-step (SS) schemes [10−12]. It can be concluded that all of these schemes are based on the sub-step procedure which results in the decrement in efficiency and accuracy. In order to alleviate such condition, Crank-Nicolson (CN) algorithm is introduced which can solve the Maxwell' equations within a single calculation procedure. The original CN scheme is merely efficient in one-dimensions [13]. By applying the original scheme to multi-dimensional problems, large sparse matrix must be calculated at each time step resulting in increment in calculation complexity. To alleviate such condition, approximate manipulation and Douglas-Gunn (DG) scheme are applied into the CN discretized form which can be denoted as the CN approximate decoupling (AD) and CNDG algorithms [14,15]. It has been testified that the CNDG algorithm shows considerable accuracy and efficiency compared with the CNAD algorithm [16,17].

In open region problems, absorbing boundary condition must be introduced to terminate the unbounded lattice [9]. The perfectly matched layer (PML) is regarded

Manuscript received December 02, 2022.
*Corresponding author.

as the most powerful and prevalent absorbing boundary condition [18]. As the original split-field scheme decreases the absorption and efficiency, unsplit-field scheme including the stretched coordinate (SC) and complex-frequency-shifted (CFS) formulation are carried out to alleviate such condition [19,20]. The SC-PML and CFS-PML schemes show advantages in terms of low-frequency evanescent waves and late-time reflections [21]. In order to further improve the performance and decrease the computation complexity, convolutional PML (CPML) scheme was introduced [22]. Due to the medium independent characteristic and considerable absorption, CPML can be regarded as one of the most powerful and prevalent absorbing boundary conditions which has been extensively employed in commercial software [23,24]. So far, the investigation on CPML implementation has become a frontier science in the field of computational electromagnetics. Meanwhile, it has been extensively employed in massive problems, such as, ground penetrating radar (GPR) problem, microwave components, and so on [25−30].

The application of PML formulation is severely limited by the medium dependent characteristic. By applying the uniform formulation to complex medium, unmatched impedance at the boundaries results in the non-absorption of outgoing waves. Among massive complex medium, magnetized plasma which holds the unique anisotropic characteristic can be regarded as one of the most important ones [31]. With the external magnetic bias, medium behaves anisotropic characteristics [32]. It shows vital importance especially in microwave components, re-entry flight and so on [33−37]. The simulation of magnetized plasma according to the FDTD algorithm can be regarded as one of the most important methods [36]. Until now, several methods have been developed to analyze the magnetized plasma in FDTD domains including the auxiliary differential equation method, recursive convolution methods and so on [38−42]. The analyzation method for rotationally symmetric structures still should be developed in BOR-FDTD scheme.

So far, it can be concluded that the simulation of rotationally symmetric structures in anisotropic magnetized plasma faces several challenges. (i) Although CN scheme have been employed in BOR-FDTD scheme to overcome the stability condition, existed algorithms cannot be directly employed into such multi-scale problem. Such condition results in the algorithm no longer valid. (ii) The simulation of anisotropic magnetized plasma in BOR-FDTD lattice still should be further investigated due to the existence of singularity point. (iii) An adequate absorbing boundary condition should be employed for the termination of anisotropic magnetized plasma. By applying existing algorithm directly, impedance unmatching results in the non-absorption of outgoing waves leading to the inaccurate solution. (iv) In the commercial CST software, the analyzation of magnetized plasma can merely be implemented through the frequency solver based on the finite element method. The absorbing boundary condition of the magnetized plasma is also limited by the conventional algorithm which results in unacceptable performance. (v) In the commercial High Frequency Structure Simulator (HFSS) software, the frequency based solver can merely accurately reflect the performance at the individual frequency point or extremely narrow frequency band.

Here, unconditionally stable CNDG algorithm is proposed in the BOR-FDTD lattice for the simulation of rotationally symmetric structures. For the unconditionally stable algorithm, an alternative method is proposed for magnetized plasma simulation in BOR-FDTD lattice with unique anisotropic characteristic. In open region problems, higher order CPML formulation is proposed which is based on the CNDG algorithm and terminates the magnetized plasma. A numerical example is carried out to illustrate the effectiveness and efficient. The results indicate that the proposed algorithm shows considerable efficiency and absorption. Meanwhile, it can overcome the CFL condition which shows significantly advantages in multi-scale problems.

2. Formulation

Inside the higher order CPML regions, two-dimensional TE_{ϕ} wave in the Maxwell's equations for BOR-FDTD algorithm can be given in the following expressions:

$$\mathrm{j}\omega E_r + \mathrm{j}\omega J_r = -S_z^{-1}\partial_z H_\phi, \tag{1}$$

$$\mathrm{j}\omega E_z + \mathrm{j}\omega J_z = S_r^{-1}\partial_r H_\phi + \frac{H_\phi}{\tilde{r}}, \tag{2}$$

$$-\mathrm{j}\omega H_\phi = S_z^{-1}\partial_z E_r - S_r^{-1}\partial_r E_z, \tag{3}$$

where E and H represent the electric and magnetic field components; J is the electric current density; r, ϕ, and z are the directions in BOR-FDTD domain; $\tilde{r}$ represents the singularity point;S_η represents the stretched coordinate variables inside the CFS-PML regions which can be given as

$$S_\eta = \kappa_\eta + \frac{\sigma_\eta}{\alpha_\eta + \mathrm{j}\omega\varepsilon_0} \tag{4}$$

where κ_η is assumed to be positive real, σ_η and α_η are assumed to be real. In (2), the operator $\tilde{r}$ represents the complex spatial coordinate stretching variables in the

BOR-FDTD domains which can be written as

$$\tilde{r} = r_1 + \int_{r_1}^{r} S_r(r')\mathrm{d}r' \tag{5}$$

where r_1 is the distance between the computational boundary and PML regions along r-direction. Equations (1)−(3) can be reorganized by employing the inverse Fourier transform (IFT) in the time domain as

$$\partial_t E_r + \partial_t J_r = -\bar{S}_z * \partial_z H_\phi, \tag{6}$$

$$\partial_t E_z + \partial_t J_z = \bar{S}_r * \partial_r H_\phi + H_\phi / \tilde{r}, \tag{7}$$

$$-\partial_t H_\phi = \bar{S}_z * \partial_z E_r - \bar{S}_r * \partial_r E_z, \tag{8}$$

where the operator $*$ represents the convolution manipulation. $\bar{S}_\eta$ is the stretched coordinate variables inside CPML regions which can be given as

$$\bar{S}_\eta(t) = \frac{\delta(t)}{\kappa_{\eta m}} + \alpha_{\eta m}(t) \tag{9}$$

where $\delta(t)$ represents the impulse function. The coefficients $\alpha_\eta(t)$ can be written as

$$\alpha_{\eta m}(t) = \beta_{\eta m} \mathrm{e}^{-\gamma_{\eta m} t} u(t) \tag{10}$$

where $\beta_{\eta m} = -\sigma_{\eta m} \Big/ \left(\kappa_{\eta m}^2 \varepsilon_0\right)$, $\gamma_{\eta m} = \alpha_{\eta m}/\varepsilon_0 + \sigma_{\eta m}/(\kappa_{\eta m}\varepsilon_0)$. The operator $u(t)$ represents the unit step function. By substituting (9) into (6)−(8) and employing the CN discretized form, they can be reorganized in the FDTD domain as

$$\begin{aligned} E_r^{n+1} =& E_r^n - p_{1ez}\varphi_{er\phi}^n - p_{2ez}\delta_z\left(H_\phi^{n+1} + H_\phi^n\right) - \\ & p_{3ez}J_r^{n+1} + p_{3ez}J_r^n, \end{aligned} \tag{11}$$

$$\begin{aligned} E_z^{n+1} =& p_{1er}\varphi_{ez\phi}^n - p_{2er}\delta_r\left(H_\phi^{n+1} + H_\phi^n\right) - \\ & p_{3er}J_z^{n+1} + p_{3er}J_z^n, \end{aligned} \tag{12}$$

$$\begin{aligned} H_\phi^{n+1} =& H_\phi^n + p_{1hr}\varphi_{e\phi z}^n - p_{1hz}\varphi_{e\phi r}^n + \\ & p_{2hr}\delta_r\left(E_z^{n+1} + E_z^n\right) - p_{2hz}\delta_z\left(E_r^{n+1} + E_r^n\right), \end{aligned} \tag{13}$$

where the coefficients can be given as $p_{1e\eta} = \dfrac{\Delta t}{\varepsilon_0}$, $p_{2e\eta} = \dfrac{\Delta t}{2\varepsilon_0\kappa_{\tilde{\eta}}}$, $p_{3e\eta} = \dfrac{\Delta t}{2\varepsilon_0}$ and $p_{1h\eta} = \dfrac{\Delta t}{\mu_0}$, $p_{2h\eta} = \dfrac{\Delta t}{2\mu_0\kappa_{\tilde{\eta}}}$. ε_0 and μ_0 represent the relative permittivity and permeability coefficients. It can be observed from (11)−(13) that two critical problems still should be addressed which include the solution of coupled field components and polarization current density at the time step n+1.

2.1 Calculation of anisotropic magnetized plasma

As can be observed from (11) and (12) that the conducing current components are coupled resulting in the invalidation of algorithm [42]. In order to alleviate such condition, an alternative algorithm for the calculation of anisotropic magnetized plasma should be investigated. Inside the magnetized plasma regions, electric current density can be given as

$$\mathrm{j}\omega J_r + \nu J_r = \varepsilon_0\omega_p^2 E_r - \omega_b J_\phi, \tag{14}$$

$$\mathrm{j}\omega J_\phi + \nu J_\phi = \varepsilon_0\omega_p^2 E_\phi + \omega_b J_r, \tag{15}$$

where the coefficients ω_b, ω_p , and ν represent the electron gyro-frequency, plasma frequency, and electron collision frequency of the magnetized plasma, respectively. Through employing (14) and (15), it can be observed that the field components are coupled. By introducing the auxiliary differential equation method, (14) and (15) can be discretized as

$$\begin{aligned} J_r^{n+1} + \frac{\nu}{2}J_r^{n+1} =& J_r^n + \frac{\nu}{2}J_r^n + \frac{\varepsilon_0\omega_p^2}{2}\left(E_r^{n+1} + E_r^n\right) - \\ & \frac{\omega_b}{2}\left(J_\phi^{n+1} + J_\phi^n\right), \end{aligned} \tag{16}$$

$$\begin{aligned} J_\phi^{n+1} + \frac{\nu}{2}J_\phi^{n+1} =& J_\phi^n + \frac{\nu}{2}J_\phi^n + \frac{\varepsilon_0\omega_p^2}{2}\left(E_\phi^{n+1} + E_\phi^n\right) + \\ & \frac{\omega_b}{2}\left(J_r^{n+1} + J_r^n\right). \end{aligned} \tag{17}$$

In order to decouple the equations, (16) is substituted into (17) and (17) is substituted into (16). One obtains

$$\begin{aligned} J_r^{n+1} =& p_1 J_r^n - p_2 J_\phi^n + p_3 E_r^{n+1} + \\ & p_3 E_r^n - p_4 E_\phi^{n+1} - p_4 E_\phi^n, \end{aligned} \tag{18}$$

$$\begin{aligned} J_\phi^{n+1} =& p_1 J_\phi^n - p_2 J_r^n + p_3 E_\phi^{n+1} + \\ & p_3 E_\phi^n + p_4 E_r^{n+1} + p_4 E_r^n, \end{aligned} \tag{19}$$

where the coefficients can be given as

$$p_1 = [1 - (\nu\Delta t/2)^2 - (\omega_b\Delta t/2)^2]/p_5,$$

$$p_2 = \omega_b\Delta t/p_5,$$

$$p_3 = [\varepsilon_0\Delta t\omega_p^2(1 + \nu\Delta t/2)]/(2p_5),$$

$$p_4 = (\varepsilon_0\Delta t^2\omega_p^2\omega_b)/(4p_5),$$

$$p_5 = (1 + \nu\Delta t/2)^2 + (\omega_b\Delta t/2)^2.$$

As can be observed from (18) and (19) that the components J_r and J_ϕ are coupled components which must be calculated simultaneously during the whole calculation procedure. By substituting these components into the discretized equations (11) and (12), one obtains

$$E_r^{n+1} = E_r^n - p_{1ez}\varphi_{er\phi}^n - p_{2ez}\delta_z\left(H_\phi^{n+1} + H_\phi^n\right) - p_{3ez}p_1J_r^n + p_{3ez}p_2J_\phi^n - p_{3ez}p_3E_r^{n+1} - p_{3ez}p_3E_r^n + p_{3ez}p_4E_\phi^{n+1} + p_{3ez}p_4E_\phi^n + p_{3ez}J_r^n, \tag{20}$$

$$E_z^{n+1} = E_z^n - p_{1er}\varphi_{ez\phi}^n - p_{2er}\delta_r\left(H_\phi^{n+1} + H_\phi^n\right) - p_{3er}p_1J_\phi^n + p_{3er}p_2J_r^n - p_{3er}p_3E_\phi^{n+1} - p_{3er}p_3E_\phi^n - p_{3er}p_4E_r^{n+1} - p_{3er}p_4E_r^n + p_{3er}J_z^n. \tag{21}$$

It can be observed that the electric field components are also coupled. Although it can be solved according to the original CN scheme, large sparse matrices must be solved at each time step resulting in the calculation much more expensive. Such circumstance leads to the unpractical simulation in large number of problems. In order to alleviate such condition, an alternative method should be investigated to decouple the coupled field components.

2.2 CNDG algorithm for magnetized plasma calculation in BOR-FDTD simulation

To calculate coupled field components, CNDG algorithm is proposed to update the entire calculation procedure. According to the CNDG algorithm, electric field components are substituted into the magnetic field components, given as

$$\begin{aligned} &H_\phi^{n+1} - p_{2er}p_{2hr}\delta_r\delta_rH_\phi^{n+1} - p_{2ez}p_{2hz}\delta_z\delta_zH_\phi^{n+1} = \\ &H_\phi^n + p_{2er}p_{2hr}\delta_r\delta_rH_\phi^n + p_{2ez}p_{2hz}\delta_z\delta_zH_\phi^n + \\ &p_{1hr}\varphi_{e\phi z}^n - p_{1hz}\varphi_{e\phi r}^n - p_{1er}p_{2hr}\delta_r\varphi_{ez\phi}^n + \\ &p_{1ez}p_{2hz}\delta_z\varphi_{er\phi}^n - p_{3er}p_1p_{2hr}\delta_rJ_\phi^n + \\ &p_{3er}p_2p_{2hr}\delta_rJ_r^n - 2p_{3er}p_3p_{2hr}\delta_rE_\phi^n - \\ &2p_{3er}p_4p_{2hr}\delta_rE_r^n + p_{3er}p_{2hr}\delta_rJ_z^n + \\ &p_{3ez}p_1p_{2hz}\delta_zJ_r^n - p_{3ez}p_2p_{2hz}\delta_zJ_\phi^n + \\ &2p_{3ez}p_3p_{2hz}\delta_zE_r^n - 2p_{3ez}p_4p_{2hz}\delta_zE_\phi^n - \\ &p_{3ez}p_{2hz}\delta_zJ_r^n + 2p_{2hr}\delta_rE_z^n - 2p_{2hz}\delta_zE_r^n. \end{aligned} \tag{22}$$

Introducing $D_{2\eta} = p_{2e\eta}p_{2h\eta}\delta_\eta\delta_\eta$ term as an auxiliary term to rewrite the equations, one obtains

$$(1 - D_{2r} - D_{2z})H_\phi^{n+1} = (1 + D_{2r} + D_{2z})H_\phi^n + A^n \tag{23}$$

where A^n represents the other field components at the time step n in (22). According to the DG scheme, (23) can be given as

$$(1 - D_{2r})H_\phi^* = (1 + D_{2r} + 2D_{2z})H_\phi^n + A^n, \tag{24}$$

$$(1 - D_{2z})H_\phi^{n+1} = H_\phi^* - D_{2z}H_\phi^n, \tag{25}$$

where H_ϕ^* is the mid-field components for updating the equations. It can be observed that the magnetic components can be updated according to (24) and (25) implicitly. Once the magnetic components are solved, the other components can be calculated explicitly. Inside the PML regions, the auxiliary variables can be given as, for example,

$$\varphi_{e\tilde{\eta}\phi}^{n+1} = b_\eta\varphi_{e\tilde{\eta}\phi}^n + a_\eta\delta_\eta\left(H_\phi^{n+1} + H_\phi^n\right) \tag{26}$$

where the coefficients can be given as

$$b_\eta = -\exp\left(\alpha_\eta + \frac{\sigma_\eta}{k_\eta}\right)\frac{\Delta t}{\varepsilon_0},$$

$$a_\eta = \frac{\sigma_\eta(b_\eta - 1)}{\kappa_\eta(\sigma_\eta + \kappa_\eta\alpha_\eta)}.$$

However, it can be observed that the value of r can be chosen as zero in the BOR-FDTD domain. According to (2), the proposed algorithm will become no longer stable in such circumstance due to the denominator infinity. In order to alleviate such condition, an alternative method for the singularity calculation should be investigated which can be given with the space mesh size discretized form as

$$\begin{aligned} E_z^{n+1}(0,k+1/2) = {} & E_z^n(0,k+1/2) - p_{1er}\varphi_{ez\phi}^n(0,k+1/2) - \\ & \frac{\Delta t}{\kappa_r\varepsilon_0}\cdot\frac{4}{\Delta r}H_\phi^n(1/2,k+1/2) - p_{3er}p_1J_\phi^n(0,k+1/2) + \\ & p_{3er}p_2J_r^n(0,k+1/2) - p_{3er}p_3E_\phi^{n+1}(0,k+1/2) - \\ & p_{3er}p_3E_\phi^n(0,k+1/2) - p_{3er}p_4E_r^{n+1}(0,k+1/2) - \\ & p_{3er}p_4E_r^n(0,k+1/2) + p_{3er}J_z^n(0,k+1/2). \end{aligned} \tag{27}$$

Through employing (27) during the singularity calculation, the entire algorithm can be implemented. As compared with the BOR-FDTD which is based on the CFS-PML scheme, the proposed algorithm shows less auxiliary variables, coefficients, and manipulators which indicates improvement in terms of efficiency and memory consumption.

3. Numerical results and discussion

Coaxial waveguide model with anisotropic magnetized plasma, dielectric bulk, and metal is proposed to demonstrate the effectiveness of the algorithm numerically. A sketch of the waveguide is shown in Fig. 1.

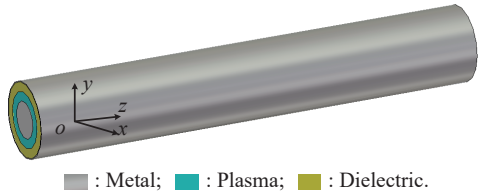

Fig. 1 Sketch of the coaxial waveguide model

As can be observed that the coaxial waveguide model is composed of metal, anisotropic magnetized plasma, dielectric bulk and metal from the inner to outer. The entire structure holds the radius and length of 4.1 mm and 50 mm. According to the BOR-FDTD algorithm, the entire three-dimensional computational domain can be converted to two-dimensions. Fig. 2 shows the sketch picture of the entire computational domain. The entire computational domain holds dimensions of 4.1 mm× 50 mm in r- and z-directions, respectively. Four layers including the metal, anisotropic magnetized plasma, dielectric, and metal locate along positive side along positive r-direction with the thickness of 2 mm, 1 mm, 1 mm, and 0.1 mm. In the calculation, the metal and dielectric materials can be expressed by the perfectly electronic conductor (PEC) and parameter of $\varepsilon_r = 4.3$, respectively. The anisotropic magnetized plasma holds the parameters of $\omega_p = 28.7\pi \times 10^9$ rad/s, $\omega_b = 10^{11}$ rads and $\nu = 20\times 10^9$ Hz.

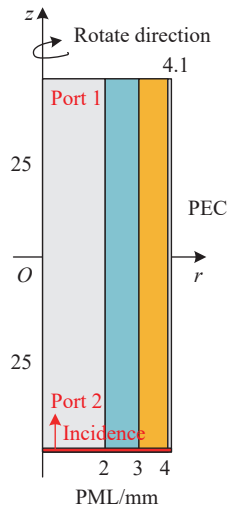

Fig. 2 Sketch picture of the coaxial waveguide model computational domain in BOR-FDTD lattice

The Port 1 and Port 2 are located at the top and bottom surface, respectively. The source radiates at the bottom from Port 2 to Port 1. The source is a Gaussian pulse with the maximum frequency of 30 GHz. The outer boundaries are terminated by PEC. The top and bottom are terminated by the 10-cell-PML regions. The observation point is located at the top right corner with the distance of one cell from both sides of the PML regions. The parameters inside PML regions are chosen to obtain the best absorption both in time domain and frequency domain. In order to compare the absorption inside different PML regions, CPML formulation based on the conventional FDTD algorithm which can be denoted as FDTD-PML in [43], CFS-PML scheme based on the CNAD scheme which can be denoted as CNAD-PML in [44] are chosen as examples for demonstration. The proposed algorithm is denoted as CNDS-PML for simplify the demonstration. It can be observed that the existences of extremely thin layer and huge difference between the width and length belong the multi-scale problem. According to the conventional FDTD scheme, uniform mesh selection and CFL stability condition limit the effectiveness of the algorithm.

In the unconditionally stable algorithm, mesh size selection can be chosen according to the calculation accuracy rather than the CFL condition. Thus, the mesh size can be chosen as $\Delta r = 0.1$ mm and $\Delta z = 1$ mm. Thus, the entire computational domain can be discretized into $41\Delta r \times 50\Delta z$. The maximum time step of the conventional FDTD algorithm can be chosen as $\Delta t_{\max}^{\mathrm{FDTD}} = 0.22$ ps. The CFL number can be defined as $\mathrm{CFLN} = \Delta t / \Delta t_{\max}^{\mathrm{FDTD}}$, where Δt is the time step in the unconditionally stable algorithm. The accuracy of the calculation can be reflected by the time domain waveform obtained by different PML algorithms and CFLNs, shown as Fig. 3.

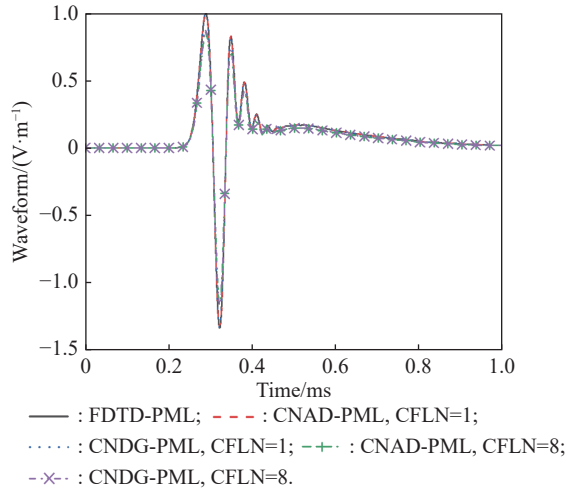

Fig. 3 Time domain waveform obtained by different PML algorithms and CFLNs at the observation point

As can be observed from Fig. 3 that the curves obtained by unconditionally stable algorithms are overlapped with the curves obtained by FDTD-PML. Such condition indicates that these algorithms hold the similar calculation accuracy with CFLN=1. With the enlargement of CFLNs, the waveforms show shifting compared with that obtained by CFLN=1. Such condition indicates that the accuracy decreases with the increment of CFLNs due to the enlargement of numerical dispersion. Compared with the CNAD algorithm, the proposed CNDG algorithm shows less shifting during the entire time domain simulation. Such circumstance indicates the pro-

posed CNDG algorithm behaviors considerable calculation accuracy.

The absorption inside PML regions can be evaluated by the relative reflection error in the time domain which can be given as

$$R_{\mathrm{dB}}(t)=20\lg\left[\frac{\left|E_r^t(t)-E_r^r(t)\right|}{\left|\max\{E_r^r(t)\}\right|}\right] \tag{28}$$

where $E_r^t(t)$ is the test solution which can be directly obtained from the observation point. $E_r^r(t)$ is the reference solution which can be obtained by the enlarged computational domain with 20 times and 128-cell-PML regions with non-changed relative distance between the source and observation point. During the calculation of reference solution, the reflection wave at the observation point can be ignored due to the existence of thick PML regions and enlarged domains. Fig. 4 shows the relative reflection error obtained by different PML algorithms and CFLNs.

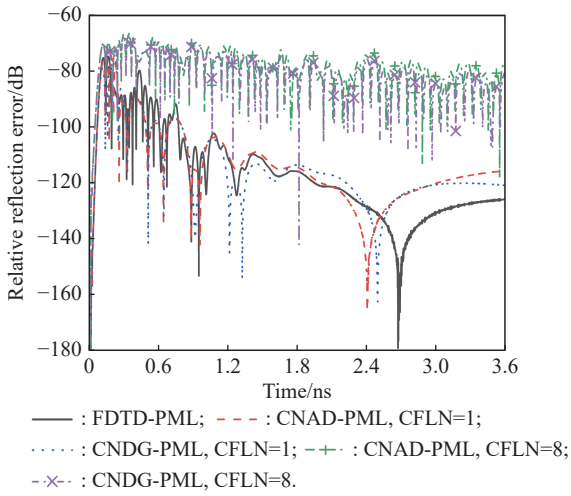

Fig. 4 Relative reflection error obtained by different PML algorithms and CFLNs

It can be observed that the conventional FDTD algorithm based CFS-PML holds the best absorption. Such condition also indicates that the conventional scheme holds the best accuracy among these schemes. Compared with CNAD-PML scheme, the proposed CNDG scheme holds the better absorption. The reason is that CNDG algorithm has the better calculation accuracy compared with the CNAD scheme due to the non-approximation manipulation. With the enlargement of CFLNs, absorption becomes worse due to the increment of numerical dispersion and calculation error. Meanwhile, it can also observe that the proposed CNDG algorithm behaves better absorption compared with the existed implicit CNAD-PML algorithm. Although the performance degenerates to −70 dB, it can still be employed in practical engineering (below −40 dB as a standard) [45]. The effectiveness can also be evaluated by the simulation duration, memory consumption, shown as Table 1.

Table 1 Comparison of CPU time, iteration steps, memory and reduction of different PML algorithms

Algorithm	CFLN	Iteration step	Time/s	Memory/MB	Reduction/%
FDTD-PML	1	65 536	21.7	2.8	−
CNAD-PML	1	65 536	84.0	3.1	−287.1
CNAD-PML	8	8 192	13.9	3.1	36.0
CNDG-PML	1	65 536	92.1	3.3	−324.4
CNDG-PML	8	8 192	15.4	3.3	29.1

As can be observed from Table 1 that conventional FDTD-PML holds the least computational resources and duration due to the explicit non-matrix calculation. The memory and duration of implicit algorithms increase significantly due to the solution of matrix during each time iteration. Compared with the CNAD algorithm, CNDG algorithm slightly increases the duration and memory during the whole simulation. Among the implicit algorithms, the calculation efficiency can be improved by employing larger CFLNs due to the employment of larger time step during the calculation.

The absorbing performance inside PML regions can also be evaluated by the reflection coefficient in the frequency domain which can be defined as follows:

$$R_{\mathrm{dB}}(f)=20\lg\left|\frac{\mathrm{FFT}\left\{E_z^t(t)-E_z^r(t)\right\}}{\mathrm{FFT}\left\{E_z^t(t)\right\}}\right| \tag{29}$$

where the operator FFT represents the fast Fourier transformation. Fig. 5 shows the reflection coefficient obtained by different PML algorithms and CFLNs in the frequency domain.

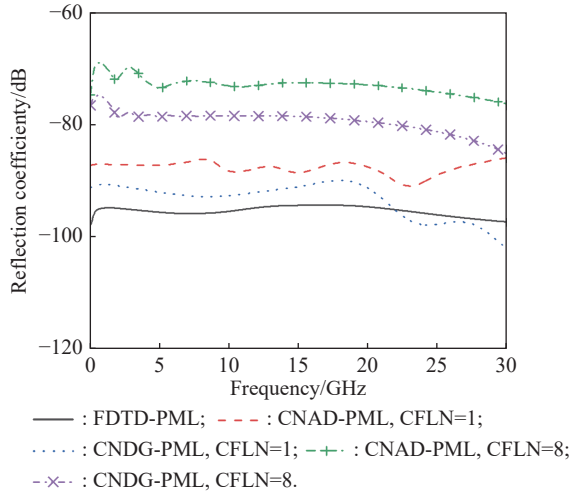

Fig. 5 Reflection coefficient obtained by different PML algorithms and CFLNs in the frequency domain

It can be observed that the conventional scheme holds the best performance through most of the entire frequency band. Compared with the CNAD algorithm, the proposed CNDG scheme improves the performance due to the enhancement of calculation accuracy. Thus, the proposed scheme behaves significantly advantage during the entire frequency band simulation. The calculation accuracy and absorption can also be reflected by the scattering parameters in the frequency domain including the return loss (S11) and transmission coefficient (S21), as shown in Fig. 6.

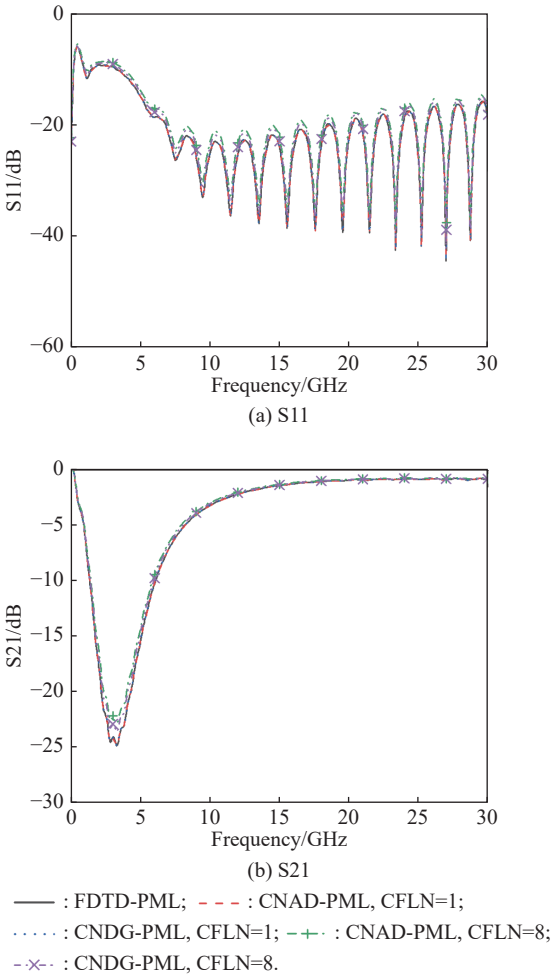

Fig. 6 Scattering parameters obtained by different PML algorithms and CFLNs in the frequency domain

Through employing these parameters, it can also draw the same conclusion that the curves obtained by different with CFLN=1 are almost overlapped which indicates the same accuracy. With the increment of CFLNs, curves show shifting compared with CFLN=1 which indicates the degeneration of calculation accuracy. However, the proposed CNDG algorithm still maintain considerable accuracy compared with the existed implicit algorithm.

4. Conclusions

An alternative CNDG-PML algorithm which is based on the CPML formulation and CNDG scheme is proposed in BOR-FDTD lattice for the anisotropic magnetized plasma simulation of rotationally symmetric multi-scale problems. At the boundaries of the lattice, CPML formulation is introduced in the proposed algorithm not only to improve the absorption but also to enhance the efficiency and memory consumption. An algorithm is proposed to efficiently analyze the magnetized plasma with unique anisotropic characteristic in the BOR-FDTD domains. In the numerical results, it can be concluded that the proposed scheme shows considerable performance during the simulation. Through converting the three-dimensional problem to 20 simulation, the proposed algorithm avoids the calculation error caused by the conformal manipulation in the conventional Yee's grid.

References

[1] YEE K S. Numerical solution of initial boundary value problems involving maxwell's equations in isotropic media. IEEE Trans. on Antennas and Propagation, 1966, 14(3): 302–307.

[2] WANG Y, WANG J, YAO L, et al. A hybrid method based on leapfrog ADI-FDTD and FDTD for solving multiscale transmission line network. IEEE Journal on Multiscale and Multiphysics Computational Techniques, 2020, 5: 273–280.

[3] WU C T, PANG Y H, WU R B. An improved formalism for FDTD analysis of thin-slot problems by conformal mapping technique. IEEE Trans. on Antennas and Propagation, 2003, 51(9): 2530–2533.

[4] OHTANI T, KANAI Y, COLE J B. A stability improvement technique using PML condition for the three-dimensional nonuniform mesh nonstandard FDTD method. IEEE Trans. on Magnetics, 2013, 49(5): 1569–1572.

[5] CHAI M, XIAO T, LIU Q H. Conformal method to eliminate the ADI-FDTD staircasing errors. IEEE Trans. on Electromagnetic Compatibility, 2006, 48(2): 273–281.

[6] SHIBAYAMA J, MURAKAMI B, YAMAUCHI J, et al. LOD-BOR-FDTD algorithm for efficient analysis of circularly symmetric structures. IEEE Microwave and Wireless Components Letters, 2009, 19(2): 56–58.

[7] WU P Y, YU H, HU Y N, et al. Approximate CN scheme and its open region problems for metamaterial rotational symmetric simulation. Journal of Systems Engineering and Electronics, 2022, 33(6): 1081–1087.

[8] ZHU D W, CHEN H L, YANG J, et al. A novel efficient WLP-based BOR FDTD method with explicit treating ideology. IEEE Access, 2019, 7: 16858–16869.

[9] TAFLOVE A, HAGNESS S C. Computational electrodynamics: the finite-difference time-domain method. Norwood: Artech House, 2005.

[10] NAMIKI T. 3-D ADI-FDTD method unconditionally stable time domain algorithm for solving full vector Maxwell's equations. IEEE Trans. on Microwave Theory and Techniques, 2000, 48(10): 1743–1748.

[11] SHIBAYAMA J, MURAKAMI B, YAMAUCHI J, et al. Efficient implicit FDTD algorithm based on locally one-dimensional scheme. Electronic Letters, 2005, 41(19): 1046–1047.

[12] KONG Y D, CHU Q X. High-order split-step unconditionally-stable FDTD methods and numerical analysis. IEEE Trans. on Antennas Propagation, 2011, 59(9): 3280–3289.
[13] STOER J, BULIRSCH R. Introduction to numerical analysis. 2nd ed. BARTELS R, GAUTSCHI W, WITZGALL C, trans. New York: Springer-Verlag, 1993.
[14] SUN G L, TRUEMAN W C. Approximate Crank-Nicolson scheme for the 2-D finite-difference time-domain method for TEz waves. IEEE Trans. on Antennas Propagation, 2004, 52(11): 2963–2972.
[15] SUN G L, TRUEMAN W C. Unconditionally stable Crank-Nicolson scheme for solving two-dimensional Maxwell 's equations. Electronic Letters, 2003, 39(7): 595–597.
[16] WU P Y, XIE Y J, JIANG H L, et al. Unconditionally stable higher order perfectly matched layer applied to terminate anisotropic magnetized plasma. International Journal of RF and Microwave Computer-Aided Engineering, 2020, 33(1): e22011.
[17] WU P Y, XIE Y J, JIANG H L, et al. Higher-order approximate CN-PML theory for magnetized ferrite simulations. Advanced Theory and Simulations, 2020, 3(4): 190021.
[18] BERENGER J P. A perfectly matched layer for the absorption of electromagnetic waves. Journal of Computational Physics, 1994, 114(2): 185−200.
[19] CHEW W C, WEEDON W H. A 3D perfectly matched medium from modified Maxwell 's equations with stretched coordinates. Microwave Optical Technology Letter, 1994, 7(13): 599–604.
[20] KUZUOGLU J M, MITTRA R. Frequency dependence of the constitutive parameters of causal perfectly matched anisotropic absorbers. IEEE Microwave Guided Wave Letter, 1996, 6(12): 447–449.
[21] BERENGER J P. Evanescent waves in PML's: origin of the numerical reflection in wave-structure interaction problems. IEEE Trans. on Antennas and Propagation, 1999, 47(10): 1497–1503.
[22] GEDNEY S D. An anisotropic perfectly matched layer-absorbing medium for the truncation of FDTD lattices. IEEE Trans. on Antennas and Propagation, 1996, 44(12): 1630–1639.
[23] LI L. Comparasion of FDTD analysis with absorbing boundary condition based on inverted-F antenna. Proc. of the 12th International Symposium on Antennas, Propagation and EM Theory, 2018. DOI: 10.1109/ISAPE.2018.8634295.
[24] FENG N X, ZHANG Y X, TIAN X Q, et al. System-combined ADI-FDTD method and its electromagnetic applications in microwave circuits and antennas. IEEE Trans. on Microwave Theory and Techniques, 2019, 67(8): 3260–3270.
[25] ZHU Y C, QIU S, LUO G X, et al. Analysis of EMP simulator with CPML. Proc. of the 4th International Conference on Intelligent Computation Technology and Automation, 2011: 451−454.
[26] ZHAI M L, YIN W Y, CHEN Z, et al. Convolution perfectly matched layer (CPML) implementation of the WCS-FDTD method for graphene applications. Proc. of the International Symposium on Electromagnetic Compatibility, 2014: 478−481.
[27] HADI M, ELSHERBENI A, PIKET-MAY M, et al. Radial waves based dispersion analysis of the body-of-revolution FDTD method. IEEE Trans. on Antennas and Propagation, 2017, 65(2): 721–729.
[28] WANG Y G, YI Y, CHEN H L, et al. An efficient Laguerre-based BOR-FDTD method using Gauss-Seidel procedure. IEEE Trans. on Antennas and Propagation, 2016, 64(5): 1829–1839.
[29] ZHANG M, LIAO C, XIONG X Z, et al. Solution and design technique for beam waveguide antenna system by using a parallel hybrid-dimensional FDTD method. IEEE Antennas and Wireless Propagation Letters, 2017, 16: 364–368.
[30] CHAHAT N, RECK T, JUNG-KUBIAK C, et al. 1.9-THz multiflare angle horn optimization for space instruments. IEEE Trans. on Terahertz Science and Technology, 2015, 5(6): 914–921.
[31] AHMED I, KHOO E H, LI E P. Development of the CPML for three-dimensional unconditionally stable LOD-FDTD method. IEEE Trans. on Antennas and Propagation, 2010, 58(3): 832–837.
[32] RODEN J A, NUTESON T W. Finite antenna array analysis and design using the FDTD technique and the CPML absorbing boundary condition. Proc. of the IEEE Antennas and Propagation Society International Symposium, 2003, 3: 776–779.
[33] FRUCHTMAN A. Thermomagnetic instability in a magnetized plasma. Physics of Fluids B: Plasma Physics, 1992, 4: 1397.
[34] ELIASSONA B, SHUKLAB P K, HALL J O. Parallel electron velocity shear instability in a magnetized plasma. Physics of Plasmas, 2006, 13: 024502.
[35] MEI J, XIE X J. Effects of a hypersonic plasma sheath on the performances of dipole antenna and horn antenna. IEEE Trans. on Plasma Science, 2017, 45(3): 364–371.
[36] BLACKWELL D D, WALKERA D N, MESSER S J, et al. Antenna impedance measurements in a magnetized plasma. II. Dipole antenna, 2007, 14: 092106.
[37] JIANG H L, XIE Y J, WU P Y, et al. Unsplit-field higher-order nearly PML for arbitrary media in EM simulation. Journal of Systems Engineering and Electronics, 2021, 32(1): 1–6.
[38] XU L, YUAN N. FDTD formulations for scattering from 3-D anisotropic magnetized plasma objects. IEEE Antennas and Wireless Propagation Letters, 2006, 5: 335−338.
[39] LI J X, WU P Y. Unconditionally stable CNAD- and BT-based CFS-PML implementation for truncating anisotropic magnetic plasma. IEEE Antenna Wireless Propagation Letter, 2018, 17(7): 1176–1180.
[40] FANG Y, XI X L, LIU J F. An iterative WLP-FDTD method for wave propagation in magnetized plasma. IEEE Trans. on Plasma Science, 2017, 45(8): 2215–2219.
[41] XU L J, YUAN N C. JEC-FDTD for 2-D conducting cylinder coated by anisotropic magnetized plasma. IEEE Microwave Wireless Component Letter, 2005, 15(12): 892–894.
[42] LIU S, LIU S B. Runge-Kutta exponential time differencing FDTD method for anisotropic magnetized plasma. IEEE Antennas and Wireless Propagation Letters, 2008, 7: 306–309.
[43] WU P Y, XIE Y J, JIANG H L, et al. Bilinear Z-transform perfectly matched layer for rotational symmetric microwave structures with magnetised ferrite. IET Microwaves, Antennas & Propagation, 2020, 14(4): 247–252.
[44] LI J X, JIAO W, ZHAO X M. Unconditionally stable CFS-PML based on CNAD-BOR-FDTD for truncating unmagnetized plasma. IEEE Trans. on Electromagnetic Compatibility, 2018, 60(6): 2069–2072.
[45] WU P, XIE Y J, JIANG H L, et al. Performance enhanced Crank-Nicolson boundary conditions for EM problems. IEEE Trans. on Antennas and Propagation, 2021, 69(3): 1513–1527.

Biographies

WEN Yi was born in 1990. She received her master's degree in instrument science and technology from University of Electronic Science and Technology of China (UESTC), Chengdu, China, in 2016. She is perusing her Ph.D. degree from UESTC. She is an engineer in Beijing Institute Aerospace Systems Engineering, Beijing, China. Her current research interests include computation electromagnetics and its application in complex media.
E-mail: luciswen@163.com

WANG Junxiang was born in 1987. He received his M.Sc. degree in instrument science and technology from the School of Automation, Northwestern Polytechnical University. He is working at Beijing Institute of Astronautical Systems Engineering. His research interests are controlled modelling and radar.
E-mail: wangjunxiang87928@126.com

XU Hongbing was born in 1966. He received his M.S. degree in automatic control from Southeast University, Nanjing, China, in 1988 and Ph.D. degree in automation from University of Electronic Science and Technology of China, Chengdu, China, in 2000. He is a professor with the School of Automation Engineering, Electronic Science and Technology of China. His research interests are intelligent information processing and control technologies.
E-mail: hbxu@uestc.edu.cn